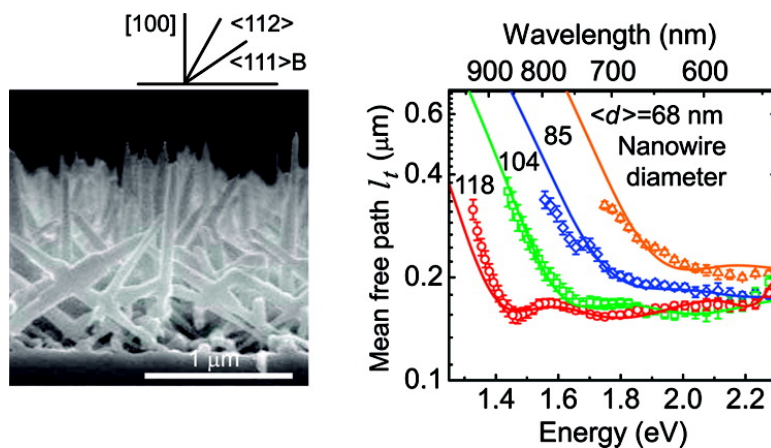


## Large Photonic Strength of Highly Tunable Resonant Nanowire Materials

Otto L. Muskens, Silke L. Diedenhofen, Bernard C. Kaas, Rienk E. Algra, Erik P. A. M. Bakkers, Jaime Gomez Rivas, and Ad Lagendijk

*Nano Lett.*, Article ASAP • DOI: 10.1021/nl802580r

Downloaded from <http://pubs.acs.org> on February 6, 2009



### More About This Article

Additional resources and features associated with this article are available within the HTML version:

- Supporting Information
- Access to high resolution figures
- Links to articles and content related to this article
- Copyright permission to reproduce figures and/or text from this article

[View the Full Text HTML](#)

# Large Photonic Strength of Highly Tunable Resonant Nanowire Materials

Otto L. Muskens,<sup>\*,†</sup> Silke L. Diedenhofen,<sup>‡</sup> Bernard C. Kaas,<sup>†</sup> Rienk E. Algra,<sup>§,||,⊥</sup>  
Erik P. A. M. Bakkers,<sup>§</sup> Jaime Gómez Rivas,<sup>‡</sup> and Ad Lagendijk<sup>†</sup>

*Center for Nanophotonics, FOM Institute for Atomic and Molecular Physics AMOLF, Kruislaan 407, 1098 SJ Amsterdam, The Netherlands, Center for Nanophotonics, FOM Institute for Atomic and Molecular Physics AMOLF, c/o Philips Research, High Tech Campus 4, 5656 AE, Eindhoven, The Netherlands, Philips Research Laboratories, High Tech Campus 4, 5656 AE, Eindhoven, The Netherlands, Materials Innovation Institute (M2i), 2628CD Delft, The Netherlands, and Institute for Molecules and Materials (IMM), Solid State Chemistry Department, Radboud University Nijmegen, Toernooiveld 1, 6525ED Nijmegen, The Netherlands*

Received August 25, 2008; Revised Manuscript Received November 11, 2008

## ABSTRACT

We demonstrate that highly tunable nanowire arrays with optimized diameters, volume fractions, and alignment form one of the strongest optical scattering materials to date. Using a new broad-band technique, we explore the scattering strength of the nanowires by varying systematically their diameter and alignment on the substrate. We identify strong Mie-type internal resonances of the nanowires which can be tuned over the entire visible spectrum. The tunability of nanowire materials opens up exciting new prospects for fundamental and applied research ranging from random lasers to solar cells, exploiting the extreme scattering strength, internal resonances, and preferential alignment of the nanowires. Although we have focused our investigation on gallium phosphide nanowires, the results can be universally applied to other types of group III–V, II–VI, or IV nanowires.

Rapid progress is being made in the development of novel functional materials based on anisotropic building blocks like nanowires<sup>1–5</sup> and nanotubes.<sup>6</sup> Nanowires exhibit novel properties of interest for applications in light emission,<sup>1</sup> biosensing,<sup>7</sup> and next-generation solar cells.<sup>2–5</sup> Light scattering is inherent to many nanostructured materials and holds promise for new approaches to light management in thin-film devices.<sup>8–11</sup> Next to its technological importance, light scattering lies at the heart of striking fundamental phenomena such as opaque superlenses,<sup>12</sup> random lasers,<sup>13</sup> and Anderson localization of light.<sup>14</sup> A continuous effort in designing new types of strongly photonic nanomaterials with tunable disorder drives many of the exciting developments in these fields.<sup>15–18</sup>

Here we assess the performance of highly tunable nanowire materials toward applications in light trapping and

Anderson localization. Through optimization of the nanowire dimensions and arrangement, we achieve a resonant nanomaterial with one of the largest scattering strengths to date. Nanowires with controlled dimensions and alignment can be grown from almost any semiconductor material on a variety of crystalline and amorphous substrates. Since nanowires consist of high-refractive index semiconductors, their strong interaction with light plays an inherently important role in their performance. For ensembles of optically thin nanowires, giant birefringence has been observed<sup>19,20</sup> resulting from the large optical anisotropy of a single wire.<sup>21</sup> For much thicker nanowires, the optical response of a single wire is governed by the internal (Mie-type) resonances of the nanowire and by antenna effects over its length.<sup>22</sup> These internal resonances correspond to the guided modes of a cylindrical wire where the light is trapped for several periods inside the nanowire.

Nanowires from the relatively wide band gap semiconductor GaP (electronic band gap at 548 nm) were chosen to unambiguously identify effects from multiple scattering without the presence of light absorption. The growth of GaP nanowires has been well characterized for various conditions and substrates.<sup>23,24</sup> Nanowires were grown using a metallo-organic vapor epitaxy following the method of ref 20. A

\* To whom correspondence should be addressed. Current address: School of Physics and Astronomy, University of Southampton, Southampton, United Kingdom; E-mail: O.Muskens@soton.ac.uk.

<sup>†</sup> Center for Nanophotonics, FOM Institute for Atomic and Molecular Physics AMOLF.

<sup>‡</sup> Center for Nanophotonics, FOM Institute for Atomic and Molecular Physics AMOLF, c/o Philips Research, High Tech Campus 4.

<sup>§</sup> Philips Research Laboratories, High Tech Campus 4.

<sup>||</sup> Materials Innovation Institute (M2i).

<sup>⊥</sup> Institute for Molecules and Materials (IMM), Solid State Chemistry Department, Radboud University Nijmegen.

**Table 1.** List of Samples with Substrate Orientations, Lateral Growth Times, Average Nanowire Diameter (Standard Deviation), Layer Thickness, Volume Fraction Estimated from SEM Images, Extrapolation Length  $z_e$ , and Mean Free Path  $l_t$  at 632.8 nm Wavelength (1.96 eV) with 95% Confidence Interval from the Fits

no.	substrate	lateral growth (s)	wire diameter (nm)	layer thickness ( $\mu\text{m}$ )	volume fraction (%)	extrapolation factor $z_e/l_t$	$l_t$ at 632.8 nm ( $\mu\text{m}$ )
1	GaP (111)B	500	43 $\pm$ 7	1.30 $\pm$ 0.1	18 $\pm$ 3	1.0	2.09 $\pm$ 0.45
2	GaP (111)B	800	59 $\pm$ 13	1.35 $\pm$ 0.1	26 $\pm$ 5	1.5	1.0 $\pm$ 0.08
3	GaP (111)B	1100	81 $\pm$ 16	1.40 $\pm$ 0.1	38 $\pm$ 5	2.5	0.41 $\pm$ 0.04
4	GaP (111)B	1400	90 $\pm$ 16	1.45 $\pm$ 0.1	50 $\pm$ 5	4.0	0.18 $\pm$ 0.02
5	GaP (111)B	1700	110 $\pm$ 18	1.50 $\pm$ 0.1	60 $\pm$ 5	6.0	0.16 $\pm$ 0.02
6	GaP (100)	500	51 $\pm$ 9	1.4 $\pm$ 0.2	17 $\pm$ 3	1.0	0.74 $\pm$ 0.07
7	GaP (100)	800	68 $\pm$ 10	1.50 $\pm$ 0.2	25 $\pm$ 5	1.5	0.23 $\pm$ 0.02
8	GaP (100)	1100	85 $\pm$ 12	1.55 $\pm$ 0.2	33 $\pm$ 5	2.0	0.19 $\pm$ 0.02
9	GaP (100)	1400	104 $\pm$ 17	1.60 $\pm$ 0.2	40 $\pm$ 5	3.0	0.16 $\pm$ 0.02
10	GaP (100)	1700	118 $\pm$ 19	1.60 $\pm$ 0.2	50 $\pm$ 5	4.0	0.16 $\pm$ 0.02
11	GaP (100)	2 $\times$ 1700	114 $\pm$ 16	4.5 $\pm$ 0.3	60 $\pm$ 5	6.0	0.20 $\pm$ 0.02

combination of vapor–liquid–solid (VLS) and lateral growth processes was used to precisely tune the diameter of the wires while keeping the nanowire density fixed. The substrates were gallium phosphide (GaP) wafers of (111)B and (100) orientations. Substrates were etched in  $\text{HNO}_3\text{:HCl:H}_2\text{O}$  (2:3:3) at 80 °C for 2 min. Immediately after this step, a gold film with a thickness of 0.3 nm was deposited on the etched surface, which was either a P-terminated (111)B or a (100) plane. Subsequently the samples were transferred to a low-pressure (50 mbar) MOVPE system (Aixtron 200). Nanowires were grown in the VLS growth mode at an elevated temperature of 420 °C using trimethylgallium (TMG) and phosphine ( $\text{PH}_3$ ) with molar fractions of  $\chi_{\text{TMG}} = 9.1 \times 10^{-5}$  and  $\chi_{\text{PH}_3} = 15.0 \times 10^{-3}$ , respectively, as precursors in a total flow of 6.0 L/min (slm) using hydrogen ( $\text{H}_2$ ) as carrier gas. Radial growth on the nanowire sidewalls was obtained by switching off TMG during a temperature ramp to 630 °C after which the TMG flow was reintroduced into the reactor. The composition of the GaP does not change during this growth step; however, relatively more lateral growth occurs at higher temperatures, compared to VLS growth. In this way the wire diameter can be changed without creating extremely long nanowires.<sup>24</sup> After growth, the samples were cooled down in a  $\text{PH}_3$  containing atmosphere.

Single-crystalline GaP nanowires grow preferentially in the  $\langle 111 \rangle$ B direction, where they have the zinc blende structure. This preferential orientation allows the wires to be aligned with respect to a crystalline substrate using epitaxial growth. Two series of materials with different nanowire orientations were fabricated by growing either on a GaP (111)B or on a GaP (100) oriented substrate. In total we have investigated 11 different materials, of which five were grown on (111)B and six on (100) substrates. A complete list of these materials is included in Table 1. A scanning electron microscope (SEM) image of a nanowire layer grown on a GaP (111)B substrate is shown in Figure 1a. This cross-sectional image shows that the nanowires are very well aligned along the vertical direction, i.e., the crystallographic  $\langle 111 \rangle$ B direction. Radial growth results in merging of nanowires and inverse tapering, leading to some irregularities in the nanowire morphology.

To characterize the scattering strength of the nanowires, we make use of enhanced backscattering (EBS) spectroscopy. EBS of light<sup>25,26</sup> is a universal and robust phenomenon which can be used for the characterization of light scattering

in any nonabsorbing material. The principle of EBS is illustrated in the inset of Figure 1b. A random material contains many multiple scattering paths that contribute to the diffuse reflectivity. Time-reversal symmetry dictates that for every path (red arrows), there is an identical path with the opposite direction (blue arrows). Light scattered along these two reciprocal paths interferes constructively in the exact backscattering direction ( $\theta = 0^\circ$ ). Away from the backscattering direction, the distribution of path lengths in the medium causes a rapid dephasing of the enhanced backscattering contribution, resulting in a cone of enhanced intensity as shown by the solid red line in Figure 1b. The center of the EBS cone is cusped because of the contribution of very long light paths involving millions of scattering events. The angular width of the cone is determined by the photonic strength  $1/k_l$ , where  $k$  denotes  $2\pi$  over the wavelength and  $l_t$  is the transport mean free path of light in the medium.

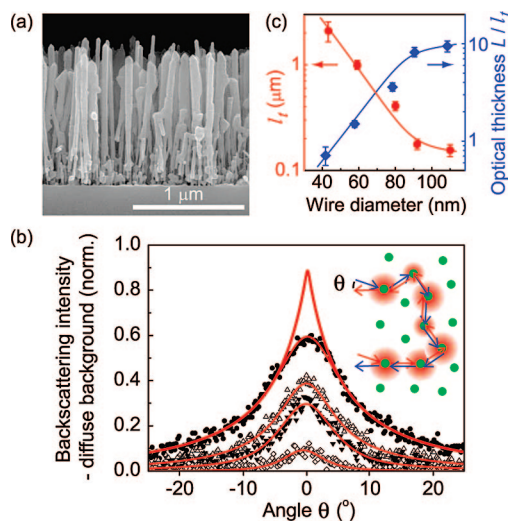


**Figure 1.** Enhanced backscattering by (111)B nanowires. (a) SEM image of GaP nanowires grown on a (111)B GaP substrate. Scale bar, 1  $\mu\text{m}$ . (b) Enhanced backscattering (EBS) cones at 632 nm wavelength of the nanowire samples with, from bottom to top, diameters increasing from 43 nm (open diamonds) to 110 nm (dots) (sample no. 1, 2, 3, 5, see Table 1). The diffuse background was subtracted for illustrative purposes. Lines (red) are fits using finite slab model. Inset shows typical reciprocal transport paths contributing to EBS. (c) Transport mean free path  $l_t$  (red dots) and optical thickness  $L/l_t$  (blue diamonds) obtained from fits; lines are guides to the eye.

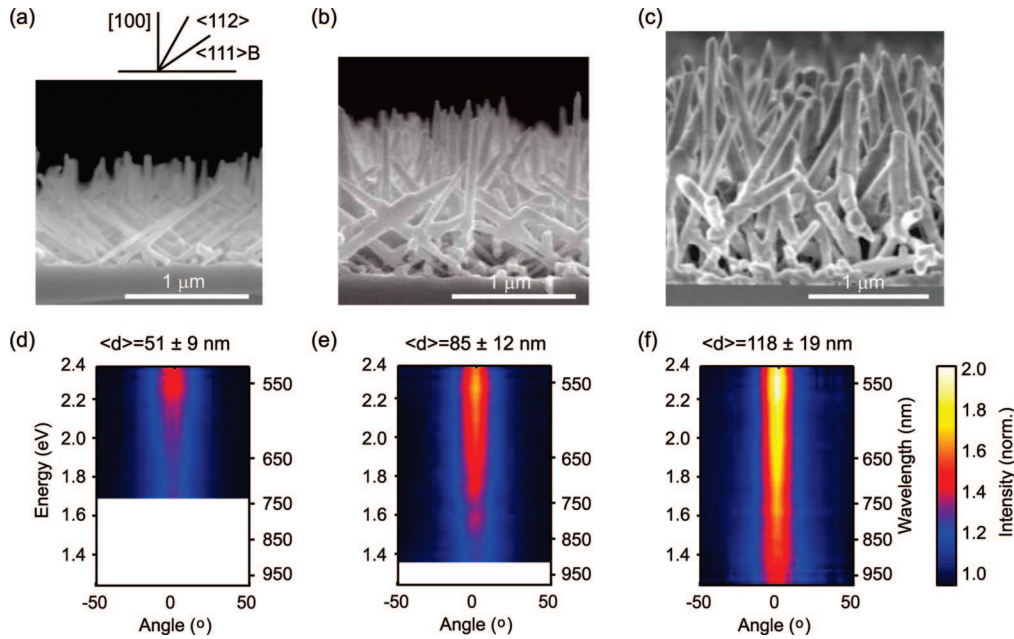


**Figure 2.** EBS spectroscopy of nanowires grown on (100) GaP. (a–c) SEM images of nanowires with increasing diameters of (a) 51, (b) 85, and (c) 118 nm (samples 6, 8, and 10, see Table 1). Scale bars, 1  $\mu\text{m}$ . (d–f) White-light-enhanced backscattering spectra of the (100) series of nanowires against photon energy (left scale) or optical wavelength (right scale). A transition from weak to strong multiple scattering is observed from (d) to (f) and from low to high energies.

Enhanced backscattering cones measured at a wavelength of 632.8 nm are shown in Figure 1b for nanowires with, from bottom to top, increasing wire diameters and volume fractions. For wire diameters below 40 nm, no coherent backscattering is observed because these samples are weakly scattering.<sup>20</sup> All cones were normalized to a Teflon reference sample with a negligible EBS contribution, after which the diffuse background was subtracted from the enhanced backscattering. This choice of normalization is most suited for visualization of the gradual buildup of the EBS cone with increasing scattering strength.<sup>27</sup> All the experimental cones in Figure 1b are rounded at their top because of the absence of very long light paths in the nanowire layers with a finite thickness. Model fits to the data are indicated by the red lines in Figure 1b, using an internal reflection correction given by the extrapolation lengths in Table 1.<sup>28</sup> These fits yield values of the transport mean free path  $l_t$  and optical thickness  $L/l_t$  of the slab as shown in Figure 1c. A continuous decrease of  $l_t$  is observed for increasing nanowire diameters, reaching a lowest value of  $0.16 \pm 0.02 \mu\text{m}$ . This mean free path is shorter than that of the most strongly scattering  $\text{TiO}_2$  powders<sup>18</sup> and comparable to that of porous GaP network materials,<sup>15,28</sup> which are two of the most strongly scattering materials at optical wavelengths. This places nanowires with optimized diameters and volume fractions among the strongest scattering materials available today.

As the nanowires preferably grow in the (111)B direction, it is possible to modify the orientation of the nanowires with respect to the surface by growing on a (100) GaP substrate. Panels a–c of Figure 2 show cross-sectional SEM images of cleaved (110) planes containing nanowires that are oriented in a number of well-defined directions. The orientational distribution indicates preferential growth in the <111>B, <112>, and [100] directions as indicated in Figure

2a. In addition to the single-wavelength measurements, we have explored the spectral variation of light scattering by the nanowires using a broad-band EBS technique specially developed for this purpose. Experimental details of this technique are presented in ref 28. Panels d–f of Figure 2 show the EBS spectra of the three nanowire materials with increasing wire diameters. The gradient of higher EBS intensity toward higher frequencies indicates an increase of the scattering strength. For layers consisting of thicker nanowires, wider EBS cones are observed over a broader frequency range. The large variations in Figure 2 between samples with different growth parameters demonstrate the tunability of the nanowire system and its interest as a novel material for optical experiments. Indications of optical resonances are weakly discernible as a small modulation on the cone widths and amplitudes in the range 1.4–1.8 eV. Much more pronounced resonant broadening of the EBS cones will be shown below for longer nanowires. To our knowledge, these measurement are the first investigation of resonant multiple scattering using broad-band EBS spectroscopy.

The broad-band EBS measurements allow a detailed comparison of the two series of nanowire materials. Values of the mean free path  $l_t$  over the entire spectral range are shown in Figure 3a for the wires grown on (111)B and (100) oriented substrates. The (100)-series of nanowires shows two regimes corresponding to a steep nonresonant variation of  $l_t$  at low photon energies and a much flatter scattering regime at high energies with an oscillating structure resulting from optical resonances. The energies at which the resonances occur depend strongly on nanowire diameter. This general behavior is reproduced well (lines in Figure 3b) by a calculation of the scattering cross sections of a collection of wires corresponding to the predominant growth directions

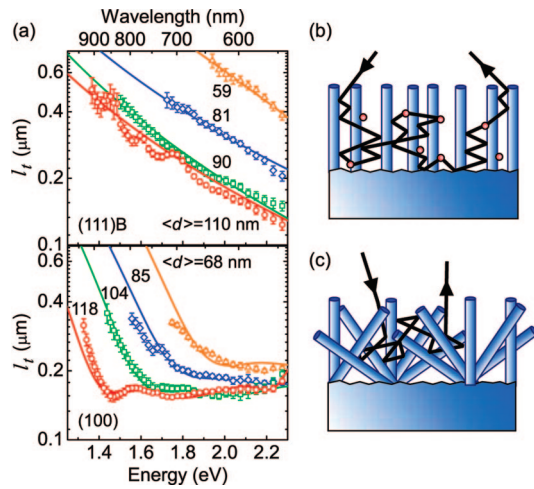


**Figure 3.** Spectral dependence of the scattering strength of nanowire materials. (a) Fitted transport mean free path  $l_t$  of GaP nanowires grown on (111)B (top, samples. 2–5) and (100) (bottom, samples 7–10, see Table 1) GaP substrates, calculated using the finite slab model. Lines for (111)B series: power-law fits with exponents ranging from  $-2.0$  to  $-2.5$ ; for (100) series: extinction calculations using the preferential orientations of Figure 2a. (b, c) Illustration of multiple scattering mechanisms in (111)B (b) and (100) (c) nanowire materials. Red dots in (b) denote isotropic point defects.

found in Figure 2, panels a–c. The nanowire density was used as a free parameter to vertically scale the curves to the experimental data. Densities of the same order but almost a factor of 2 smaller than the experimental values were found. This discrepancy is most likely attributed to screening of the single-wire cross section by the surrounding nanowires.<sup>29</sup> The above single-wire calculations however serve as an illustration of the resonant scattering properties of the nanowire materials.

In comparison with the (100) series of nanowire materials, the (111)B series in Figure 3a shows a remarkably different scattering behavior over the entire spectral range. The mean free path follows a monotonous decrease with increasing energies that can be fit (lines) to a power law with exponents ranging between  $-2.0$  and  $-2.5$ . At energies around 2 eV,  $l_t$  depends much stronger on nanowire diameter for the (111)B than for the (100) nanowires. As we will describe below, this strong dependence of the scattering strength on wire diameter can be explained by the strong anisotropy of the scattering cross section of the aligned (111)B nanowires, which in the vertical direction is ultimately limited by small deviations from the ideal wire shape.

The differences between the two nanowire materials are attributed to the preferential orientations of the wires, as is illustrated in Figure 3, panels b and c. For a single nanowire, momentum conservation along the cylindrical axis results in a cone of forward scattered radiation. For the (100) series of nanowires, the distribution of wire orientations rapidly leads to efficient randomization of the incident light as illustrated in Figure 3c. For the (111)B series, where the nanowires are aligned along the vertical direction, propagation along the wire axis is ballistic and diffusion only takes place in the two perpendicular dimensions (see Figure 3b).

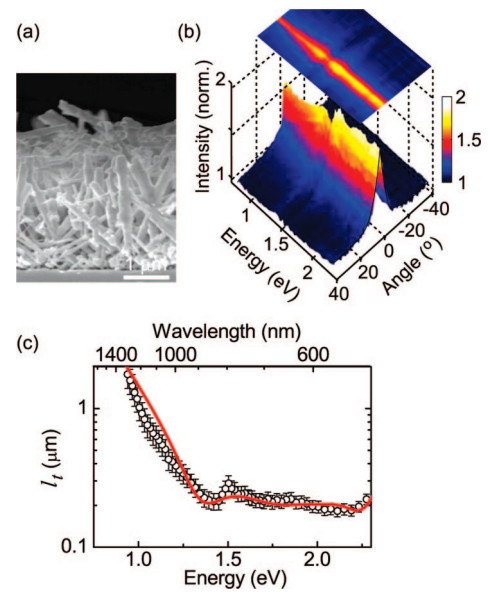


**Figure 4.** Investigation of strongly scattering, compressed nanowire material. (a) SEM image of the compressed nanowire layer (sample no. 11, see Table 1). Scale bar 1  $\mu\text{m}$ . (b) EBS spectrum from 0.9 to 2.2 eV of a 4.5  $\mu\text{m}$  thick nanowire layer. Internal nanowire resonances are observed as a modulation of the width and amplitude around 1.4 eV. A projection of the EBS spectrum is shown in the color-density map above (b). (c) Fitted values of  $l_t$  (circles, black) with (red line) calculation of  $l_t$  similar to Figure 3a.

Nanowire materials like those in Figure 1a, however, do not consist of perfect cylinders but contain a large density of imperfections which give rise to randomization of light. These imperfections have a morphology and therefore a mean free path different from the cylindrical nanowires. The mixture of aligned nanowires and point defects as shown in Figure 3b can be described analogous to the problem of absorption in a diffusive medium, where the imperfections play the role of absorption sites. In such a model, the effective transport length will depend on the square root of the isotropic randomization length (see, e.g., ref 11). For isotropic Rayleigh scatterers and a flat nanowire dispersion, this model description results in an inverse quadratic dependence of the mean free path on energy as is the case for the (111)B series in Figure 3a.

As the nanowires of this study form one of the strongest scattering media available at optical wavelengths, explorations of possible effects of Anderson localization may be within reach. Such experiments will however have to be performed on much thicker nanowire layers which still is technologically challenging. As a first step, we have obtained longer nanowires with controlled thickness by alternating VLS and lateral growth steps for several times. To enhance the density of the layer, the nanowire layer was gently compressed between sapphire plates. This resulted in a nearly close-packed layer of nanowires of around 4.5  $\mu\text{m}$  thickness, as shown in the SEM image of Figure 4a. The EBS spectrum of this layer, measured over the entire visible and near-infrared range from 0.9 to 2.25 eV, is shown in Figure 4b, with a mean free path obtained from fits shown in Figure 4c. The increased length of the nanowires provides an optical thickness up to  $L/l_t = 25$ , resulting in sharp EBS cones that

are visible far into the infrared spectral region, where the nanowires are weakly scattering. Around 1.4 eV, a modulation of  $I_t$  due to the presence of internal nanowire resonances is observed which is in quantitative agreement with that of the thickest, 1.5  $\mu\text{m}$  long nanowires in Figure 3a. This agreement confirms that the resonances result from guided modes over the nanowire diameter rather than from antenna resonances over the nanowire length.<sup>22</sup>

The strong presence of resonant scattering effects in the nanowire layers is remarkable given their large diameter dispersion. Usually, resonant effects require much more monodisperse colloidal systems. The survival of resonant scattering effects in the diffuse transport regime is also highly nontrivial since it involves a complicated averaging over all possible directions and orientations. Resonant transport has been observed only recently in  $\text{TiO}_2$  photonic glass and in weakly scattering colloidal suspensions.<sup>16,17</sup> The survival of nanowire scattering resonances is more pronounced in the case of (100) wires because the relevant length scale is governed by the resonant nanowires in all three dimensions, rather than in two dimensions as for the (111)B wires.

The combination of a large scattering strength with strong resonances of nanowire materials holds promise for light trapping applications. Multiple light scattering can fold the absorption length many times in a random walk, making it a strategic tool for achieving efficient light absorption in thin-film devices.<sup>11</sup> The large variation of the scattering strength of nanowires near the resonance regime can be optimized for specific light harvesting molecules to improve energy conversion in dye-sensitized solar cells.<sup>9,10</sup> For devices in which nanowires form the active layer,<sup>3–5</sup> trapping of light inside the high-index nanowire at an internal resonance will provide a significant increase of the effective absorption length.<sup>30</sup> The alignment of nanowires forms an interesting new tuning parameter for maximizing the effective path length by anisotropic scattering.

In conclusion, we have demonstrated that semiconductor nanowires with highly tunable structural properties form one of the most strongly scattering materials to date. Using a broad-band EBS technique, we have identified strong internal resonances of the nanowires in the scattering mean free path. Effects of preferential alignment of nanowires with respect to the substrate were found and explained in terms of a simplified anisotropic scattering model. Our results open up new prospects for experiments in light transport in random media using nanowires and for applications in light trapping for photovoltaic energy conversion.

**Acknowledgment.** We acknowledge T. van der Beek, E. Evens, I. Mijnders, G. Immink, and W. van der Einden for their technical support and P. M. Johnson for fruitful discussions and for help with the calculations. This work is part of the research program of the “Stichting voor Fundamenteel Onderzoek der Materie (FOM)”, which is financially

supported by the “Nederlandse Organisatie voor Wetenschappelijk Onderzoek (NWO)”, and is part of an industrial partnership program between Philips and FOM.

## References

- (1) Huang, M. H.; Mao, S.; Feick, H.; Yan, H.; Wu, Y.; Kind, H.; Weber, E.; Russo, R.; Yang, P. *Science* **2001**, *292*, 1897–1899.
- (2) Law, M.; Greene, L. E.; Johnson, J. C.; Saykally, R.; Yang, P. *Nat. Mater.* **2005**, *4*, 455–459.
- (3) Peng, K.; Xu, Y.; Wu, Y.; Yan, Y.; Lee, S.-T.; Zhu, J. *Small* **2005**, *1*, 1062–1067.
- (4) Tsakalacos, L.; Balch, J.; Fronheiser, J.; Korevaar, B. A.; Sulima, O.; Rand, J. *Appl. Phys. Lett.* **2007**, *91*, 2331171:3.
- (5) Goodey, A. P.; Eichfeld, S. M.; Lew, K.-K.; Redwing, J. M.; Mallouk, T. E. *J. Am. Chem. Soc.* **2007**, *129*, 12344–12345.
- (6) Yang, Z.-P.; Ci, L.; Bur, J. A.; Lin, S.-Y.; Ajayan, P. M. *Nano Lett.* **2008**, *8*, 446–451.
- (7) Cui, Y.; Wei, Q.; Park, H.; Lieber, C. M. *Science* **2001**, *293*, 1289–1292.
- (8) Nishimura, S.; Abrams, N.; Lewis, B. A.; Halaoui, L. I.; Mallouk, T. E.; Benkstein, K. D.; Van de Lagemaat, J.; Frank, A. J. *J. Am. Chem. Soc.* **20003**, *125*, 6306–6307.
- (9) Ito, S.; Zakeeruddin, S. M.; Humphry-Baker, R.; Liska, P.; Charvet, R.; Comte, P.; Nazeeruddin, M. K.; Péchy, P.; Takata, M.; Miura, H.; Uchida, S.; Grätzel, M. *Adv. Mater.* **2006**, *18*, 1202–1205.
- (10) Zhang, Q.; Chou, T. P.; Russo, B.; Jenekhe, S. A.; Cao, G. *Adv. Funct. Mater.* **2008**, *18*, 1654–1660.
- (11) Muskens, O. L.; Diedenhofen, S.; Kaas, B. C.; Algra, R. E.; Bakkers, E. P. A. M.; Gómez Rivas, J. *Nano Lett.* **2008**, *8*, 2638–2642.
- (12) Lerosey, G.; de Rosny, J.; Tourin, A.; Fink, M. *Science* **2007**, *315*, 1120–1122.
- (13) Wiersma, D. S. *Nat. Phys.* **2008**, *4*, 359–367, and references therein.
- (14) Schwartz, T.; Bartal, G.; Fishman, S.; Segev, M. *Nature* **2007**, *446*, 52–55.
- (15) Gómez Rivas, J.; Lagendijk, A.; Tjerkstra, R. W.; Vanmaekelbergh, D.; Kelly, J. J. *Appl. Phys. Lett.* **2002**, *80*, 4498–4500.
- (16) Reufer, M.; Rojas-Ochoa, L. F.; Eiden, S.; Sáenz, J. J.; Scheffold, F. *Appl. Phys. Lett.* **2007**, *91*, 171904–171906.
- (17) Sapienza, R.; García, P. D.; Bertolotti, J.; Martín, M. D.; Blanco, Á.; Vina, L.; López, C.; Wiersma, D. S. *Phys. Rev. Lett.* **2007**, *99*, 233902: 1–4.
- (18) Störzer, M.; Gross, P.; Aegerter, C.; Maret, G. *Phys. Rev. Lett.* **2006**, *96*, 063904:1–4.
- (19) Muskens, O. L.; Borgström, M. T.; Bakkers, E. P. A. M.; Gómez Rivas, J. *Appl. Phys. Lett.* **2006**, *89*, 2331171:3.
- (20) Muskens, O. L.; Diedenhofen, S. D.; Borgström, M. T.; Bakkers, E. P. A. M.; Gómez Rivas, J. *Adv. Funct. Mater.* **2008**, *18*, 1039–1046.
- (21) Wang, J.; Gudiksen, M. K.; Duan, X.; Cui, Y.; Lieber, C. M. *Science* **2001**, *293*, 1455–1457.
- (22) Chen, G.; Wu, J.; Lu, Q.; Gutierrez, H. R.; Xiong, Q.; Pellen, M. E.; Petko, J. S.; Werner, D. H.; Eklund, P. C. *Nano Lett.* **2008**, *8*, 1341–1346.
- (23) Borgström, M. T.; Immink, G.; Ketelaars, B.; Algra, R.; Bakkers, E. P. A. M. *Nat. Nanotechnol.* **2007**, *2*, 541–544.
- (24) Verheijen, M. A.; Immink, G.; De Smet, T.; Borgström, M. T.; Bakkers, E. P. A. M. *J. Am. Chem. Soc.* **2006**, *128*, 1353–1359.
- (25) van Albada, M. P.; Lagendijk, A. *Phys. Rev. Lett.* **1985**, *55*, 2692–2695.
- (26) Wolf, P.-E.; Maret, G. *Phys. Rev. Lett.* **1985**, *55*, 2696–2699.
- (27) van der Mark, M. B.; van Albada, M. P.; Lagendijk, A. *Phys. Rev. B* **1988**, *37*, 3575–3592.
- (28) Muskens, O. L.; Lagendijk, A. *Opt. Express* **2008**, *16*, 1222–1231.
- (29) Kirchner, A.; Busch, K.; Soukoulis, C. M. *Phys. Rev. B* **1997**, *57*, 277–288.
- (30) van Tiggelen, B. A.; Lagendijk, A.; van Albada, M. P.; Tip, A. *Phys. Rev. B* **1992**, *45*, 12233–12243.

NL802580R